*Tellus* (1986), *38A*, 263–276

# The influence of baroclinicity and stability on the wind and temperature conditions at the Georg von Neumayer Antarctic station

By CHRISTOPH KOTTMEIER, *Institut für Meteorologie und Klimatologie, der Universität Hannover, Herrenhäuser Straße 2, D-3000 Hannover 21, FRG*

(Manuscript received June 4; in final form October 8, 1985)

ABSTRACT

The situation that arises when a stably stratified layer of air exists over a large inclined surface is examined using a resistance law formulation for baroclinic conditions. The dependence of the surface wind direction on the surface Rossby number, the stability parameter $S$ and the angle between the geostrophic wind direction and the vector of largest inclination is obtained. For slope angles typical for the coastal areas of eastern Antarctica, the surface wind direction is mainly determined by the static stability of the air mass through its thermal wind effects, while its stabilizing effect on turbulent motion is less important for boundary layer wind veering. Consequently a simpler analytic formula can be derived which is able to describe the features of the flow direction with respect to the free atmospheric geostrophic wind and the temperature deficit within the boundary layer. Synoptic data from the Georg von Neumayer Antarctic Station obtained in 1983 are discussed using the theoretical results. The comparison of theory and observations clearly suggests that the observed relationships between the wind speed, the wind direction and the temperature can only be explained when a strong baroclinicity at the antarctic coast is taken into account.

## 1. Introduction

This paper discusses some properties of the stably stratified planetary boundary layer above an inclined terrain, when the isothermal surfaces are parallel to the ground and the angle of surface inclination to the horizontal surface is small and does not vary horizontally.

This situation was first considered by Prandtl (1942), who assumed the absence of Coriolis forces and free-flow geostrophic wind. He formulated the classical slope wind theory. Other theories, for instance by Mahrt and Schwerdtfeger (1970), have been developed to take the influence of the Coriolis force into account. They, however, assumed an eddy viscosity constant with height, and this has been shown by Deardorff and Mahrt (1982) to be insufficient for describing the shear stress profile. Ball (1956) presented a theory of katabatic flows for elevation angles of 0.01 and more, in which case the effect of earth's rotation leads only to a slight deviation of the surface wind direction to the fall line of about 8–12°.

Mahrt (1982) put forward a scheme that put order into previous theories. He incorporated a maximum time scale for the flow to neglect Coriolis effects. He did not try, however, to take large-scale flows into consideration when this time scale is exceeded. Gutman and Melgarejo (1981) have presented resistance laws which take the baroclinic effects into account, which occur due to the horizontal temperature gradients when the planetary boundary layer air over an inclined surface possesses a temperature deficit when compared to the overlying free atmospheric flow. They show that even a small inclination angle $\psi$ of $3 \cdot 10^{-3}$ is sufficient to have an appreciable influence on the heat and momentum transfer in the boundary layer.

The theoretical formulation of Gutman and Melgarejo (1981) will be used to discuss the dependence of the surface wind direction on the

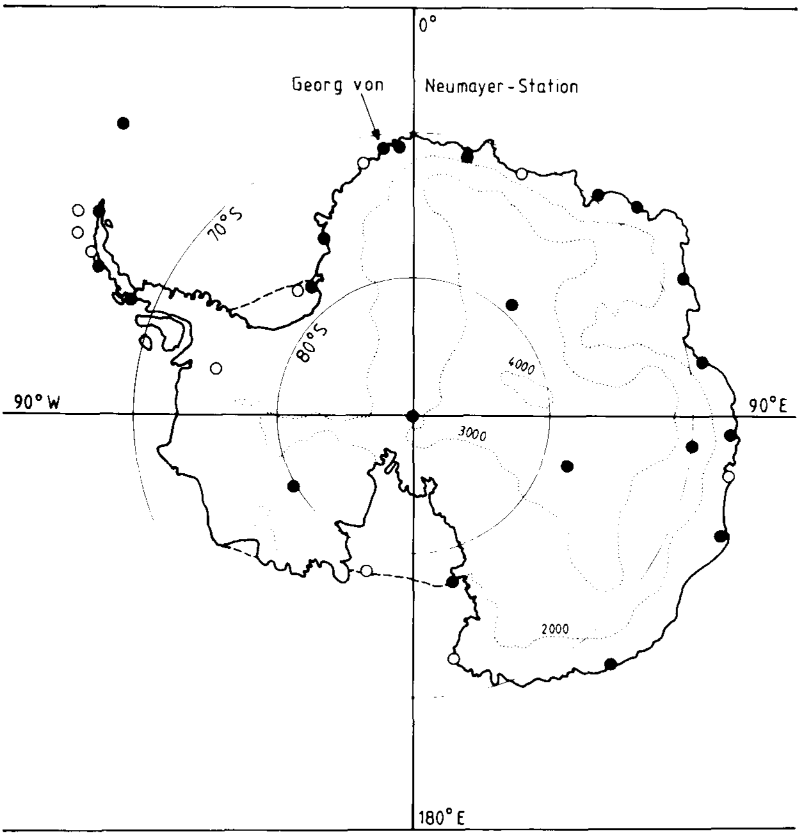


*Fig. 1.* Map of Antarctica and the stations, which operated at least for two years (closed circles), but not in 1968 (open circles) and the Georg von Neumayer-Station. After Landsberg (1970).

geostrophic wind speed $G$, the geostrophic wind direction $\chi$ and the temperature deficit $\Delta\theta$ between the surface air temperature and the temperature at the boundary layer top. The results of the resistance law application will be compared with a simpler theoretical formulation. Climatic data obtained at the Georg von Neumayer Antarctic station will then be discussed with respect to the theoretical results. Fig. 1 shows a map of Antarctica and the location of the Georg von Neumayer station.

## 2. Coordinates and notation

The situation to be considered is that of a stably stratified planetary boundary layer over an infinite surface which is inclined to the horizontal surface at an angle $\psi$ (Fig. 2a). At the height of the stable layer $h$, the potential temperature is by $\Delta\theta$ higher than at the surface. The free flow geostrophic wind at the top of the PBL is given by a constant $G$. The isothermal surfaces are assumed to be parallel to the ground.

Fig. 2b shows the definition of the angles $\chi$, $\alpha$ and $\delta$ in a right-handed cartesian system, where $x$ is directed down the slope, $y$ perpendicular to it and $z$ upward. $\chi$ denotes the angle of the free-flow geostrophic wind, $\alpha$ the angle between the surface stress $\tau$ and the geostrophic wind $G$. $\delta$ gives the angle between $\tau$ and the $x$-axis. A list of notation is given in the Appendix V.

## 3. Resistance law formulation

Gutman and Melgarejo (1981) were able to develop resistance laws for the situation described

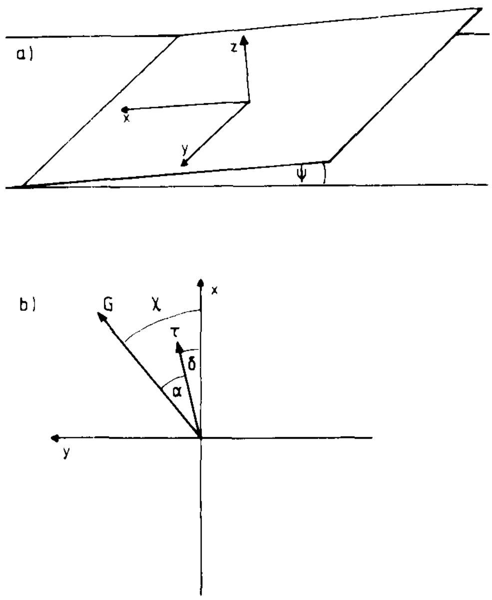


*Fig. 2.* Notation of angles and coordinates on a sloping plane.

above, where the laws depend on three empirical functions $A(\mu)$, $B(\mu)$ and $C(\mu)$. The baroclinic effects are incorporated by additional terms into the three resistance laws containing $\chi$ and $\psi$.

Their formulations contrasts with those of others, e.g., Wippermann (1973), who also considered baroclinic influences and obtained an additional dependence of the empirical functions $A$, $B$ and $C$ on baroclinic factors $\lambda_x$ and $\lambda_y$, while the resistance laws remained unchanged.

Some external influences can be combined to give two nondimensional parameters, the surface Rossby number

$$\mathrm{Ro} = \frac{G}{|f| z_0}, \tag{1}$$

and the stability parameter

$$S = \frac{g}{\theta} \frac{\Delta\theta}{|f| G}. \tag{2}$$

Gutman's and Melgarejo's results can be applied as follows. For given values of $\chi$, $\psi$ and $\mu$, the geostrophic drag coefficient $u_*/G$ can be calculated by an iteration scheme from

$$\ln \mathrm{Ro} = B - \ln \frac{u_*}{G} + \left[ \left\{ \frac{\kappa G}{u_*} \sin\chi + \frac{(B-C)\,\mu\psi}{\kappa^2} \right\}^2 + \left\{ \frac{\kappa G}{u_*} \cos\chi + \frac{A\mu\psi}{\kappa^2} \right\}^2 - A^2 \right]^{0.5}, \tag{3}$$

which is valid for small angles $\psi \ll 10^{-2}$. The above formula can be simplified in the barotropic case $\psi = 0$) to give the well-known resistance law for barotropic conditions.

The cross-isobaric angle α was shown by the authors to obey

$$\sin\alpha = \frac{1}{b_3} \left[ A - b_4 \frac{A b_4 - b_3 (B - \ln(\mathrm{Ro}\, u_*/G))}{A^2 + (B - \ln(\mathrm{Ro}\, u_*/G))^2} \right]^2. \tag{4}$$

α can be calculated in dependence on $\chi$, $\tau$ and $\mu$, when $u_*/G$ is given by (3). To give a dependence on $S$ instead of $\mu$, the third resistance law

$$\left| \frac{T_*}{\Delta\theta} \right| = \left[ \ln\left( \mathrm{Ro} \frac{u_*}{G} \right) - C - b_5 \right]^{-1} \tag{5}$$

must be solved. In (4), (5) and (6) the functions $b_3$, $b_4$, and $b_5$ are defined by

$$b_3 = \frac{kG}{u_*} + ((B-C)\sin\chi + A\cos\chi)\frac{\mu\psi}{\kappa^2},$$

$$b_4 = ((B-C)\cos\chi - A\sin\chi)\frac{\mu\psi}{\kappa^2}, \tag{6}$$

$$b_5 = ((B-C)\sin\delta - A\cos\delta)\left(\frac{\kappa N}{f}\right)^2 \frac{\psi}{\mu}.$$

Using the equation

$$S = \frac{\mu u_* \Delta\theta}{k^3 G T_*}, \tag{7}$$

sin α can finally be computed in terms of $\chi$, $\psi$, Ro and $S$ (or $\Delta\theta$). The functions $A(\mu)$ and $B(\mu)$ given by Gutman and Melgarejo (1981) and $C(\mu)$ according to Zilitinkevichs (1975) data were used during the calculation. In order to determine the angle α from eq. (4), it was necessary to develop a criterion as to whether the main or secondary values of the arcussinus-function were valid. This was done by the independent solution of an additional equation for the function tan α which can be derived from Gutman and Melgarejos, eqs. (35) and (38).

## 4. Results with the aid of the resistance laws

Calculations have been made for an angle $\psi = 5 \cdot 10^{-3}$, which can be regarded as realistic for the slopes of Antarctica near the Georg von Neumayer Antarctic station (8°22′ W, 70°37′ S). Fig. 3 shows five meridional cross-sections near the antarctic coast between 10° W and 10° E. The topography gradient in this area is directed approximately to NNW, which means that in this case the $x$-axis is directed to 340° and the $y$-axis to 250°.

An inclination of $5 \cdot 10^{-3}$ can be assumed only for flows of a typical length scale of 500 km to 1000 km. Flows of smaller length scales will be effected much more by the local terrain features, which can be very different from the assumption above. The Georg von Neumayer station, for instance, is situated on the Ekström iceshelf with typical dimensions of 100 km and an inclination of $10^{-3}$.

A roughness length of $1.7 \cdot 10^{-4}$ has been used, which corresponds to the local $z_0$ of the Ekström iceshelf given by König (1985) for neutral stratification. An effective roughness length as proposed by Fiedler and Panofsky (1972) was not available due to the absence of data on vertical velocity standard deviations.

The results of the calculations are given in the following figures, where the angle $\delta$ is shown in dependence on the stability parameter $S$ and the geostrophic wind direction $\chi$. Each of the solid lines corresponds to a constant value of $\chi$, the parameter lines denote values of $\chi$ between −175° to +195° in steps of 10°. A diagram of this kind is only valid for a specified Rossby number, but the dependence on Ro will be shown to be only of a slight nature.

Fig. 4 shows the results for the barotropic case ($\psi = 0$). The angle α in this case is independent of $\chi$. The angle $\delta$ decreases with increasing stability in the Southern Hemisphere, since the cross isobaric angle increases with increasing stability. For higher values of $S$, the cross isobaric angle becomes more and more independent of $S$, so the isolines of constant $\chi$ become parallel to the $x$-axis. The boundary layer wind veering with respect to stability roughly assumes values between 10° and 30°. That is why a wind direction near the ground is much more dependent on the geostrophic wind direction than on stability. Under baroclinic conditions (Fig. 5) this statement no longer holds. When a critical value of $S$ is exceeded, the surface wind direction undergoes an abrupt change. Being nearly independent of the given $\chi$-value, all lines tend towards $\delta$-values within a small range around 72°. This corresponds to a wind direction deviating 18° to the right from the terrain contour lines. The effect can be attributed to the change of the surface geostrophic wind direction with increasing stability, i.e., to the increasing thermal wind.

The Rossby number specified in Fig. 5 can be regarded as a very high value, corresponding to

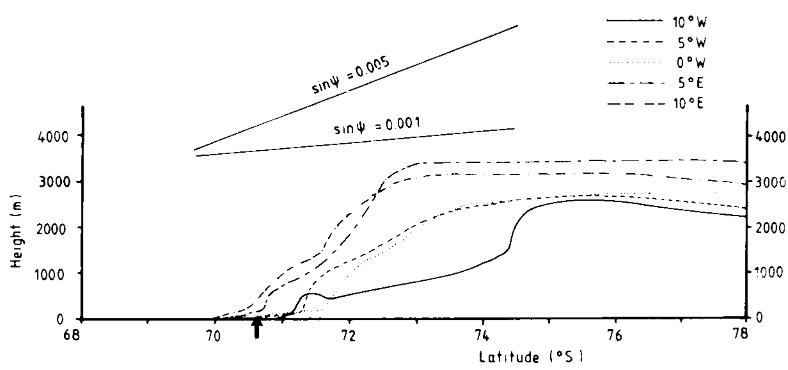


*Fig. 3.* Five meridional cross-sections of the topography at the coast of Antarctica. The arrow denotes the latitude of the Georg von Neumayer Antarctic station, whose longitude is 8°22′ W. The straight lines give inclinations of 0.001 and 0.005.

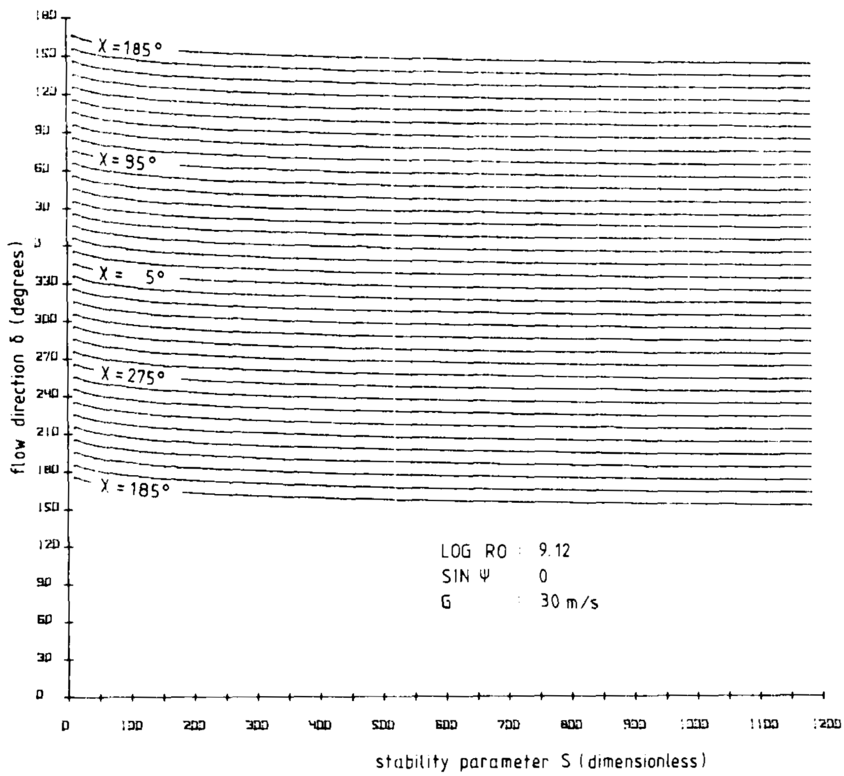


*Fig. 4.* Barotropic solutions for the flow direction $\delta$ in dependence on the geostrophic wind direction $\chi$ and stability $S$, valid for a constant geostrophic wind speed of 10 m/s and roughness length of $1.7 \cdot 10^{-4}$ m. Calculations based on the resistance laws.

$G = 30$ m/s and $z_0 = 1.7 \cdot 10^{-4}$. The results for smaller Rossby numbers which are not shown here, however, differ only slightly in a universal diagram like Fig. 5.

## 5. Simplified analysis by means of an analytical formula

The results obtained by applying the resistance laws lead to the conclusion that the surface wind direction under strong baroclinic conditions is much more dependent on the thermal wind than on frictional effects and on the free-flow geostrophic wind. Thus it was hoped that the main feature of the dependencies could be modelled by a simpler analysis. Using the same coordinates and notations as given above, the equations of motion can be written

$$fv - fv_{g,h} = \frac{\partial}{\partial z}\overline{w'u'} - g\frac{\Delta\theta}{\theta_0}\sin\psi, \tag{8}$$

$$-fu + fu_{g,h} = \frac{\partial}{\partial z}\overline{w'v'}, \tag{9}$$

where the last term in (8) gives the height-dependent part of the pressure gradient force due to the stable stratification above inclined terrain. The components of the free-flow geostrophic wind are defined as usual by

$$v_{g,h} = \frac{1}{\rho f}\frac{\partial p}{\partial x}\bigg|_h, \tag{10}$$

$$u_{g,h} = -\frac{1}{\rho f}\frac{\partial p}{\partial y}\bigg|_h. \tag{11}$$

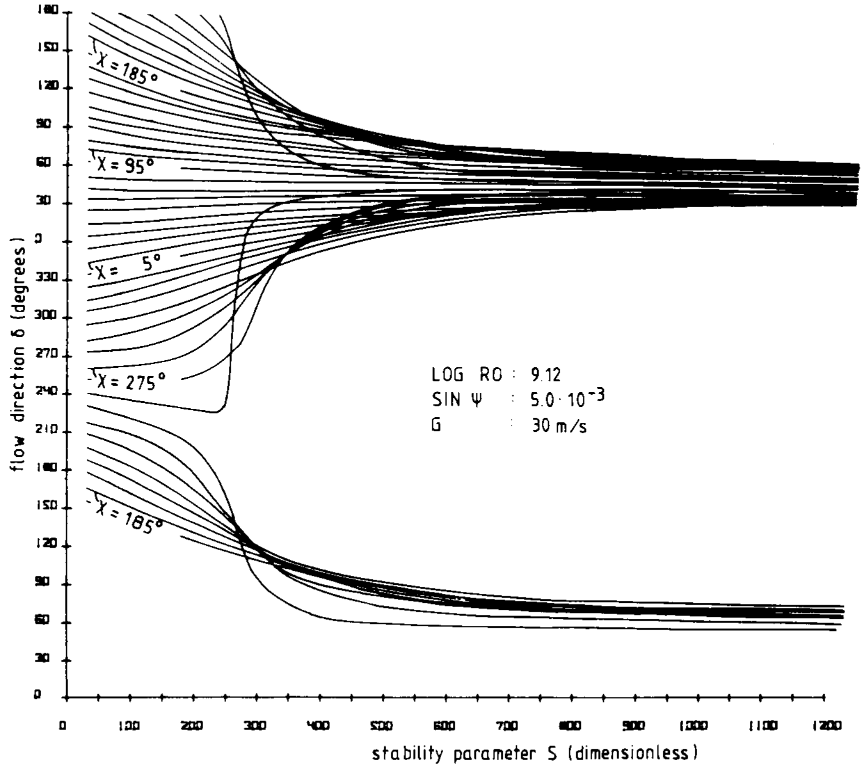


*Fig. 5.* Baroclinic solutions for the flow direction $\delta$ in dependence on the geostrophic wind direction $\chi$ and stability $S$, valid for a constant geostrophic wind speed of 30 m/s and roughness length of $1.7 \cdot 10^{-4}$ m. Calculations based on the resistance laws.

The surface stress components are assumed to follow a quadratic drag law

$$\overline{w'u'_0} = -c_d \frac{u_{10}^2}{\cos\delta}, \tag{12}$$

$$\overline{w'v'_0} = -c_d \frac{u_{10}^2}{\sin\delta}, \tag{13}$$

which is based on the assumption that the total surface stress is proportional to the square of the velocity at a height of 10 m. As in the previous chapter, a roughness length of $z_0 = 1.7 \cdot 10^{-4}$ m, calculated by König (1985) from the neutral profiles, was used. Under neutral conditions, this $z_0$-value corresponds to a drag coefficient of 0.001, when $z$ is 10 m. This value of $c_D$ was used for all stabilities. The height of the boundary layer is estimated by

$$h = a_1 \frac{\kappa u_{*,0}}{|f|}, \qquad a_1 < 1, \tag{14}$$

where $a_1$ is a numerical factor and smaller than unity, which takes into account that the above relation with $a_1$ equal to unity holds only for neutral stratification. Investigations by Arya (1981) showed a correlation of 0.68 between observed and calculated stable boundary layer heights, when $a_1 = 0.36$. The stress terms in (8) and (9) need a determination of the stress profiles gradient. Using eq (12) to (14) the gradients of both stress components can be written as

$$\frac{\partial}{\partial z}\overline{w'u'} = a_2 \frac{c_d u_{10}^2}{\cos\delta}\frac{|f|}{a_1 \kappa u_{*,0}}, \tag{15}$$

$$\frac{\partial}{\partial z}\overline{w'v'} = a_2 \frac{c_d u_{10}^2}{\sin\delta}\frac{|f|}{a_{1\kappa} u_{*,0}} \tag{16}$$

where $a_2$ is a factor, which has to be considered when the stress gradients in the reference level of 10 m differ from the mean stress gradients of the layer, which would be given by $-\overline{w'u'_0}/h$ and

$-\overline{w'v_0'}/h$. In general the stress profiles shows a stronger curvature near the ground than above, so that $a_2$ is larger than 1. The variety of observations and numerical model results concerning stable boundary layers show that $a_2$ is far from constant for different stabilities and boundary layer heights. The calculations have been made by varying factors $a_2$. They led to the result that the surface wind direction is much less sensitive to a change in $a_2$ than to different stabilities. So the assumption of a constant factor $a_2$ seems to be justified for the present study. The computation of other boundary layer variables, however, must not be carried out using this assumption about frictional effects.

Combining the two constants $a_1$ and $a_2$ by a single parameter $a = a_2/a_1$ and with the eqs. (15) and (16), the equations of motion can be written

$$fv_{10} - fv_{g,h} = \frac{a\sqrt{c_d}\,|f|\,u_{10}}{\kappa} - g\frac{\Delta\theta}{\theta}\sin\psi, \tag{17}$$

$$-fu_{10} + fu_{g,h} = \frac{a\sqrt{c_d}\,|f|\,v_{10}}{\kappa}. \tag{18}$$

The abbreviations

$$z_1 = \frac{u_{g,h}}{v_{g,h} - \dfrac{g}{f}\dfrac{\Delta\theta}{\theta}\sin\psi} \tag{19}$$

$$z_2 = \frac{a\sqrt{c_d}}{\kappa} \tag{20}$$

are useful for giving an analytic solution for the cross isobar angle. $z_1$ gives the ratio of the near-surface geostrophic wind components, showing that only the slope-parallel component is affected by the specified inversion strength. $z_2$ represents the frictional effects, which depend on

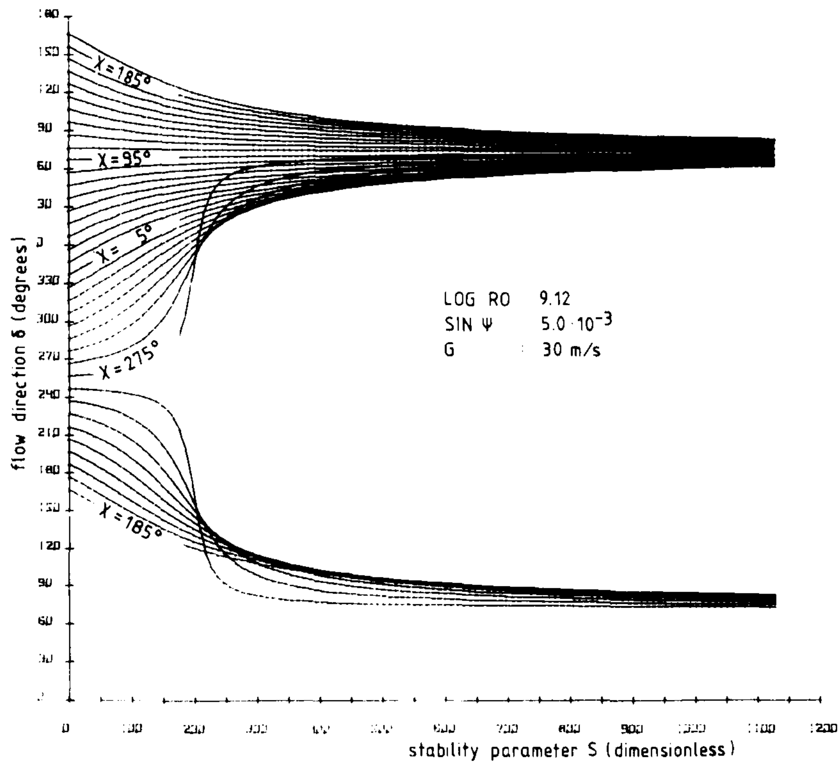


*Fig. 6.* Solutions for the flow direction $\delta$ in dependence on the geostrophic wind direction $\chi$ and the stability parameter $S$, valid for a constant geostrophic wind speed of 10 m/s and roughness length of $1.7 \cdot 10^{-4}$ m. Calculations based on formula (21).

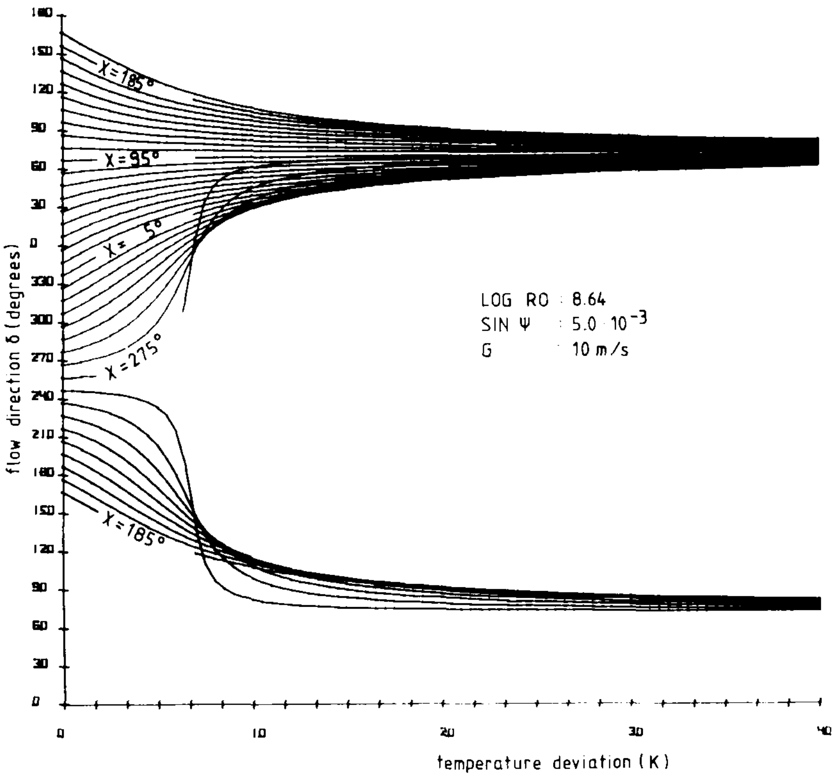


*Fig. 7.* Solutions for the flow direction $\delta$ in dependence on the geostrophic wind direction $\chi$ and horizontal temperature deviation $\Delta\theta$ valid for a constant geostrophic wind speed of 10 m/s and roughness length of $1.7 \cdot 10^{-4}$ m. Calculations based on formula (21).

the chosen values of $c_d$ and $a$. Finally, the solution for the angle $\delta$ is given by

$$\tan\delta = \frac{v_{10}}{u_{10}} = \frac{1 - z_1 z_2}{z_1 + z_2}. \tag{21}$$

For specified values of the free-flow geostrophic wind speed and wind direction, of the inclination and $\psi$ and the temperature deficit $\Delta\theta$, $\delta$ can be calculated from (21). To calculate the wind direction, the parameter a needs to be specified. From eqs. (19) to (21) it is clear, that $\tan\delta$ is equal to $z_2^{-1}$ for a geostrophic wind exactly parallel to the slope, since $u_g = 0$ in this case. $\tan\delta = z_2^{-1}$ is also a limit for strong stability, when the slope induced pressure gradient dominates both components of the external pressure gradient so that $z_1 \to 0$. The limiting value from the resistance laws for this case is $\tan\delta = 3.08$, when the $A$, $B$, $C$-functions of Gutman and Melgarejo (1981) are used. Assuming this limit, the constants $a$ and $a_2$ are given by

$$a = 4.1,$$

$$a_2 = a_1 a = 0.36 \cdot 4.1 = 1.5$$

The derivation of (21) has been done for the height of 10 m which corresponds to the surface stress direction of the resistance laws. The difference can be considered to be small, since the wind direction will not change very much in the lowest 10 m. Thus the results of this chapter can be compared with those of the previous chapter.

Fig. 6 shows the results for the same assumptions as in Fig. 5. A comparison of both figures makes sure that the main features of the stability-dependent surface wind direction have been successfully determined by the analytic solution. There is a slight difference in the exact value of $S$ where the flow direction starts to undergo a considerable change. This can be

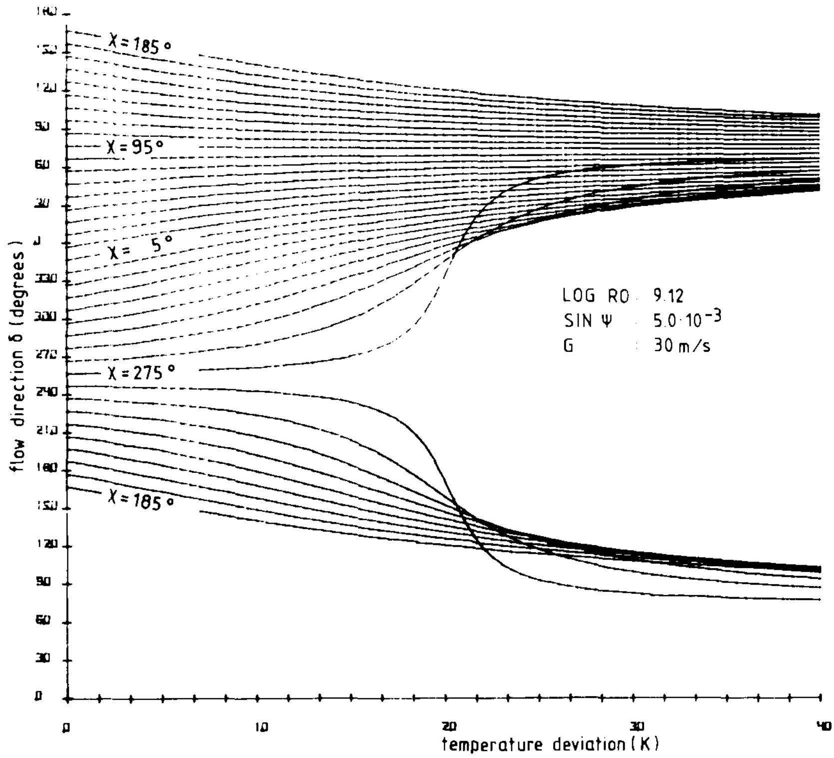


*Fig. 8.* Solutions for the flow direction $\delta$ in dependence on the geostrophic wind direction $\chi$ and horizontal temperature deviation $\Delta\theta$ valid for a constant geostrophic wind speed of 30 m/s and roughness length of $1.7 \cdot 10^{-4}$ m. Calculations based on formula (21).

ascribed to the different empirical assumptions that are used in both methods. Two further figures are given, which show the dependence of $\delta$ on $\Delta\theta$ instead of $S$. This has been done in order to discuss measurements when $G$ is unknown. Figs. 7 and 8 demonstrate that the onset of thermal wind-induced wind veering (i.e. the abrupt change of constant-$\chi$ lines) occurs in strong dependence on $G$. The weaker the free flow geostrophic flow, the more important thermal wind effects become. For small values of $G$, the "forbidden" region of surface wind directions is much larger than for large values of $G$.

This means physically that the slope-introduced pressure gradient exceeds the external pressure gradient so that the wind no longer can flow uphill and can have only a small downhill component.

## 6. Discussion of data with respect to the theoretical results

A favourable site for a frequent occurrence of the situation described above seems to be the site of the Georg von Neumayer Antarctic station. The southern hemisphere cyclones usually travel around Antarctica to the east, but they are hardly able to reach the inland areas of the continent except over the Weddell Sea and the Ross Sea. Their paths can be more or less distant from the continent, giving cause for more or less intense warm air advection. Climatic conditions, see for instance Landsberg (1970), show that in July the meridional surface temperature gradient is rather constant between 70° S and 40° S, while in January the maximum temperature gradient can be found between 50° S and 40° S. It may be concluded that in the winter months the warm air advection towards the continent in front of moving cyclones is much more intense even when the cyclone's origin was only slightly north of Antarctica. When warm air is transported towards the steeply rising flanks of Antarctica, a stabilization of the air from below has to be expected.

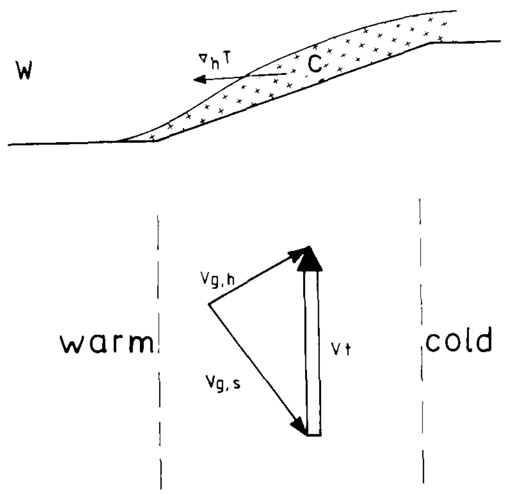


*Fig. 9.* Schematic thermal wind conditions at the coast of Antarctica and the resulting relationship between geostrophic and thermal winds.

Fig. 9 shows the schematic situation for periods of intense warm air advection which affects a horizontal temperature gradient when the cooling reaches an almost constant height above the surface everywhere. The relation between an assumed geostrophic wind vector, the terrain-induced thermal wind and the resulting surface geostrophic wind is given in the lower portion of the figure. Since the thermal wind is directed to the east, the surface geostrophic wind will gain an increasing component parallel to the slope, depending on the magnitude of the temperature deficit. Climatic data from the Georg von Neumayer station seem to be a convenient data source for discussing the possible situations near the antarctic coast in relation to the theoretical results.

The situation sketched in Fig. 9 is similar to that discussed by Schwerdtfeger (1975) for the eastern flanks of the Antarctic peninsula. Schwerdtfeger assumed the development of the thermal wind due to the advection of cold air from the Weddell Sea.

Fig. 10 shows the relation between the surface wind direction and the surface wind speed (both at a height of 10 m) for the winter period of 1983. Fig. 11 gives the relation between the surface wind direction and the "characteristic" temperature difference $\Delta T$. $\Delta T$ has been determined as the difference between the actual temperature $T$ at a height of 2 m and the first harmonic temperature wave of the year. $\Delta T$ can be regarded as a strong indicator for the intensity of warm air advection towards the continent or advection of cold air away from the continent. The variation of $\Delta T$ with time is highly correlated with the pressure and the wind speed variations on a time scale of several days and has to be considered as mainly influenced by synoptic scale advection and not by local heating or cooling.

Due to the lack of direct measurements of the actual horizontal temperature gradients, another approach seems to be justified. We consider the minimum of $\Delta T$, which is approximately $-12$ K, to correspond to the origin of the $\Delta\theta$-scale. Except this constant offset both scales are assumed to be identical. That means physically, that the coldest periods have no significant horizontal temperature gradient over the flanks of the continent. The warmest periods, however, have the strongest cross antarctic temperature gradient, determined by the measured potential temperature near the shelf ice edge and the potential temperature in the interior of the continent, which can be measured during the outflow situation at that time of the year. The author is aware of the the possible inaccuracy of the above assumption, but a hypothesis consistent with observations, as will be shown below, seems to be of appreciable value until a better theory or better measurements are available.

The position of the Georg von Neumayer station about 100 km north of the steepest slopes is favourable in this context, since warm air masses are able to reach its site, causing a temperature change. Sites further south have to be expected to show less distinct variations of the temperature near the ground.

The data points in Fig. 10 can be divided into four groups. The first represents wind directions between 120 degrees and 210 degrees, all of which occur with wind speeds of less than 8.5 m/s. In the period under consideration data points in group 1 make up 21% of all data. The same wind directions in Fig. 10 are accompanied by $\Delta T$-values over the range between $-11$ K and $+11$ K. With respect to Figs. 7 and 8 and assuming $\Delta T$ to represent $\Delta\theta$ as a first guess, most of the data of this group occupy a "forbidden" region when assuming $G = 10$ m/s and they match theory only for $G > 20$ m/s. High values of $G$ of 20 m/s in these cases are improbable, however, since the surface winds were rather calm.

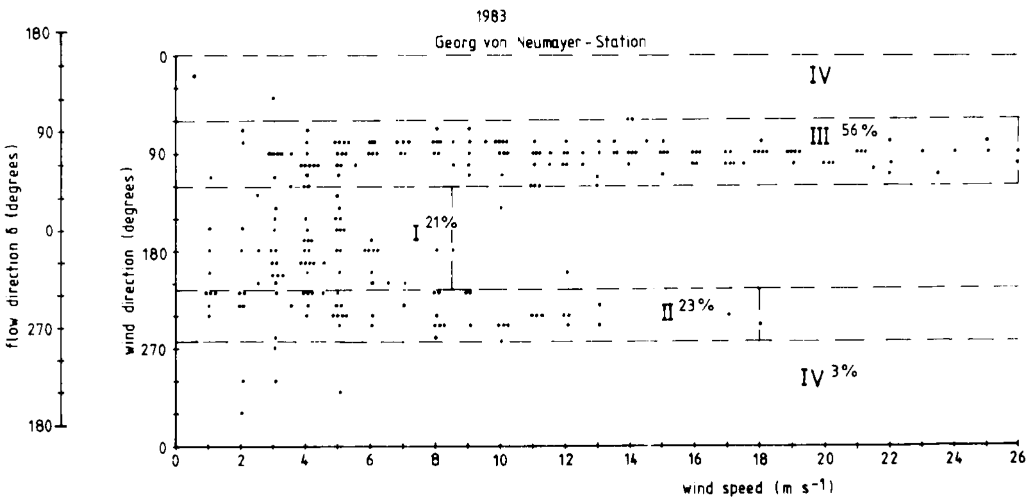


*Fig. 10.* Relationship between wind direction (10 m) and wind speed at the Georg von Neumayer station between February and December 1983. Each dot represents one day of the period. The second vertical axis corresponds to the coordinate system of theoretical considerations. Dashed lines give limits of data classes.

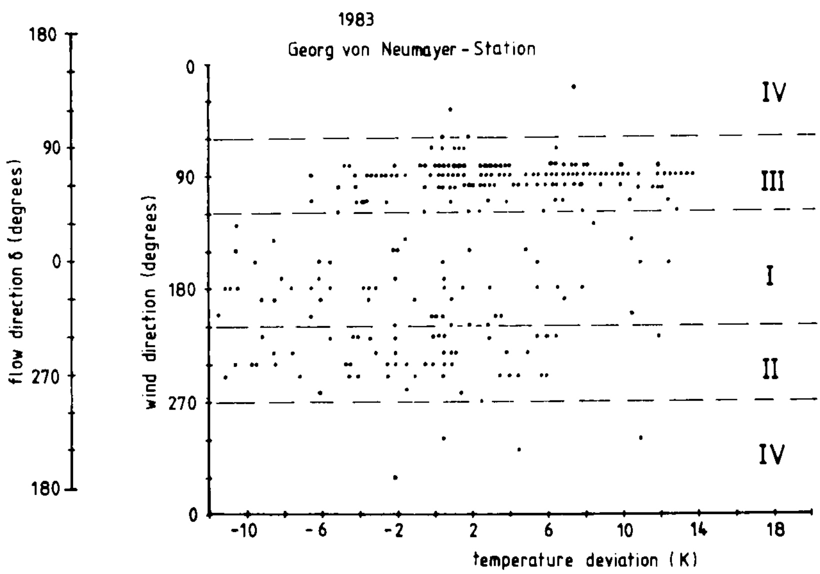


*Fig. 11.* Relationship between wind direction and temperature (in terms of deviation from first harmonic temperature wave) at the Georg von Neumayer station between February and December 1983. Each dot represents one day of the period. The second vertical axis corresponds to the coordinate system of theoretical considerations. Dashed lines give limits of proposed data classes.

We can discuss the data of group 1 by considering Fig. 12, which gives a sketch of a cyclone at the antarctic coast. Both for the barotropic case and in relation to Fig. 10, we have to conclude that the free-flow geostrophic wind came from the southern sector. This means that the measurements have been made on the cold side of a cyclone or of an anticyclonic ridge. In this sector of

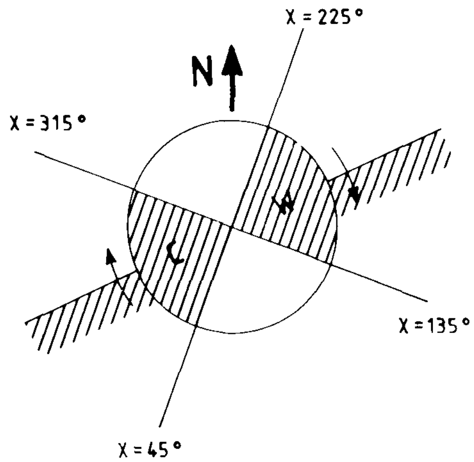


*Fig. 12.* Sketch of a cyclone at the coast of Antarctica near 0°W and sectors favourable for warm and cold air advection.

a pressure system cold air is transported to lower latitudes and the situation described by the theory is very unlikely to occur. Thus there is no disagreement between theory and observations. The synoptic situations providing data points of group 1 can roughly be described as situations of katabatic flows. A detailed study of these katabatic flows has been prepared by Kottmeier (1986).

The second data group with about the same frequency as group 1 situations is given by the rather small range of directions between 210° and 270°. The mean wind speed was 8 m/s and the maximum wind speed 18 m/s. Taking Figs. 7 and 8 into account, the data of Fig. 11, group 2, are only consistent with high values of *G*. In these cases the geostrophic wind, according to theory, was westerly. This leads us to expect that these measurements were made when a cyclone passed south of the Georg von Neumayer station, leading to a geostrophic wind from the west. Cyclones passing that far south, and consequently near the steep slopes of the continent, were probably intense cyclones with strong geostrophic winds. This conclusion supports the results of the theory, which demands strong geostrophic winds in these cases, too. The weaker surface winds are consistent with theory as well, since the thermal wind is directed to the east and weakens the surface wind.

Group 3 data of Figs. 10 and 11 are characterized by wind speeds up to 26 m/s and represent 56% of all data. For wind speeds of more than 15 m/s almost 96% of the synoptic situations are combined with easterly winds, within a very small range at the surface. Fig. 11 shows that there is an obvious correlation between high temperatures and easterly winds. The data of group 3 are completely consistent with theory (Fig. 9) for all values of *G*. They can be considered as highly affected by the strong baroclinicily at the antarctic coast when warm air advection occurs. Any attempt to explain the climatic data at the Georg von Neumayer station without baroclinic influences as described above would lead to a more open distribution of wind directions, which would represent more or less the distribution of the free-flow geostrophic wind directions.

Group 4 data, which occupy directions between 270 degrees and 60 degrees, are statistically unimportant. The few data points of this sector are combined with calm winds and seem to be of no climatic importance. Due to the calm winds the *T* data in this group will have been mainly affected by local heating or cooling.

The almost complete lack of data from this group can be interpreted as follows. The sector of cyclones favourable for geostrophic NW-, N- and NE-winds is the sector with strongest warm air advection. According to Fig. 6 and the definition of *S* (eq. 2) in these situations the flow is parallel to the contour lines (e.g. easterly) up to stronger external pressure gradients when compared to other situations with a weaker slope induced pressure gradient.

## 7. Concluding remarks

The above explanation of near-surface synoptic data at the Georg von Neumayer station leads to some additional conclusions of further significance. The strong thermal wind effects will not only influence the surface wind direction, but also the surface wind speed. It will produce a low-level jet stream in many cases. This jet stream will be most pronounced, when the thermal wind is strong, i.e., when there is strong warm air advection, and when at the same time the free-flow geostrophic wind is from the east. For approaching cyclones the thermal wind effects can explain the steering effect near the antarctic coast which means the orientation of isobars parallel to the slope of Antarctica. The analyses of Antarctic synoptic charts are frequently made by estimating the pressure gradient from the near-surface wind data. This method holds for the surface pressure field, but there is a possibility of misleading conclusions being drawn. The pressure field constructed from wind data can alter its direction within a few hundred meters above the surface, so that a near-surface easterly wind may correspond to a westerly geostrophic wind above.

In addition to these consequences, an adjustment of the pressure field in response to the acceleration in front of approaching depressions can be expected.

A quantitative discussion of these effects is planned for the future and will be supported by the radiosonde data from the Georg von Neumayer station.

## 8. Acknowledgements

The author wishes to thank his colleagues H. J. Belitz and H. U. Stuckenberg of the wintering team at the Georg von Neumayer station in 1983 for providing the synoptic data. He is also grateful to Prof. R. Roth for helpful discussions, to J. Melgarejo for his comments in an earlier state of the work, and to A. Tiedemann and R. Hartig for their assistance.

## 9. Appendix

| | |
|---|---|
| $A(\mu)$, $B(\mu)$, $C(\mu)$ | universal functions of the resistance laws (defined as in Gutman and Melgarejo (1981)) |
| $f$ | Coriolis parameter |
| $G$ | free-flow geostrophic wind speed |
| Ro | surface Rossby number |
| $S$ | temperature stratification parameter |
| $T_*$ | friction temperature |
| $u_*$ | friction velocity |
| $a_1$ | dimensionless parameter of the boundary layer height formula (eq. 14) |
| $a_2$ | dimensionless parameter due to the curvature of the stress profile (eqs. (15, 16)) |
| $a$ | ratio of $a_2$ and $a_1$ ($a = a_2/a_1$) |
| $c_D$ | drag coefficient ($c_D = (u_*/u_{10})^2$) |
| $h$ | height of the stable layer near the ground |
| $u_{g,h}$, $v_{g,h}$ | downslope and cross-slope geostrophic wind components at the height $h$ |
| $x$, $y$, $z$ | cartesian coordinates as defined in Fig. 2 |
| $z_0$ | roughness length |
| $\alpha$ | angle between the surface stress and the free-flow isobars |
| $\delta$ | angle between the surface stress and the $x$-axis |
| $\Delta\theta$ | potential temperature deficit |
| $\theta$ | mean potential temperature |
| $\mu$ | stratification parameter $\left(\mu = \dfrac{\kappa^3 g T_*}{f - u_*}\right)$ |
| $\chi$ | angle between the geostrophic wind and the $x$-axis |
| $\psi$ | terrain inclination angle |
| $\tau$ | surface stress |
| $\kappa$ | von Karman constant ($\kappa = 0.4$) |
| $\lambda_x$, $\lambda_y$ | baroclinic parameters in Wippermanns (1973) notation |
| $N$ | stratification parameter (see Gutman and Melgarejo, 1981) |
| $b_3$, $b_4$, $b_5$, $z_1$, $z_2$ | abbreviations for longer expressions, meaning given in the text |

REFERENCES

Arya, S. P. S. 1981. Parameterizing the height of the stable atmospheric boundary layer. *J. Appl. Meteorol.* *20*, 1192–1202.

Ball, F. K. 1956. The theory of strong katabatic winds. *Aust. J. Phys.* *9*, 373–386.

Deardorff, J. W. and Mahrt, L. 1982. On the dichotomy in theoretical treatments of the atmospheric boundary layer. *J. Atmos. Sci.* *9*, 2096–2098.

Fiedler, F. and Panofsky, H. 1972. The geostrophic drag coefficient and the effective roughness length. *Q. J. R. Meteorol. Soc.* *98*, 213–220.

Gutman, L. N. and Melgarejo, W. 1981. On the laws of geostrophic drag and heat transfer over a slightly inclined terrain. *J. Atmos. Sci.* *38*, 1714–1724.

König, G. 1985. Roughness length on an Antarctic ice shelf. *Polarforsch.* in press.

Kottmeier, Ch. 1986. Shallow gravity flows over the Ekström ice shelf. *Boundary Layer Meteorol. 34*, no. 3.

Landsberg, H. E. 1970. Climates of the polar regions. On: *World survey of climatology*, vol. 14. Amsterdam-London-New York: Elsevier Publishing Company.

Mahrt, J. and Schwerdtfeger, W. S. 1970. Ekman spirals for exponential thermal wind. *Boundary Layer Meteorol. 1*, 137–145.

Mahrt, L. 1982. Momentum balance of gravity flows. *J. Atmos. Sci. 39*, 2701–2711.

Prandtl, L. 1942. *Führer durch die Strömungslehre.* Braunschweig/Germany: Verlag Vieweg und Sohn, pp. 373–375.

Schwerdtfeger, W. 1975. The effect of the Antarctic peninsula on the temperature regime of the Weddell Sea. *Mon. Wea. Rev. 103*, 45–51.

Wippermann, F. 1973. The planetary boundary layer of the atmosphere. *Ann. Meteorol. 7* (Neue Folge) 1–346.

Zilitinkevich, S. S. 1975. Resistance laws and prediction equations for the depth of the planetary boundary layer. *J. Atmos. Sci. 32*, 741–752.